Tailoring Electroactive β- and γ-Phases via Synthesis in the Nascent Poly(vinylidene fluoride) Homopolymers

Yogesh Patil, Jiayi Zhao, Bruno Ameduri, Sanjay Rastogi

Tailoring electroactive β- and γ-phases via the synthesis in the nascent poly(vinylidene fluoride) homopolymers

Yogesh Patil[1], *Jiayi Zhao*[1], *Bruno Ameduri*[2] *and Sanjay Rastogi*[1*]

[1] Physical Sciences and Engineering (PSE) Division, King Abdullah University of Science and Technology (KAUST), Thuwal 23955, Saudi Arabia.

[2] Institut Charles Gerhardt, CNRS, University of Montpellier, ENSCM, Montpellier, 34095, France.

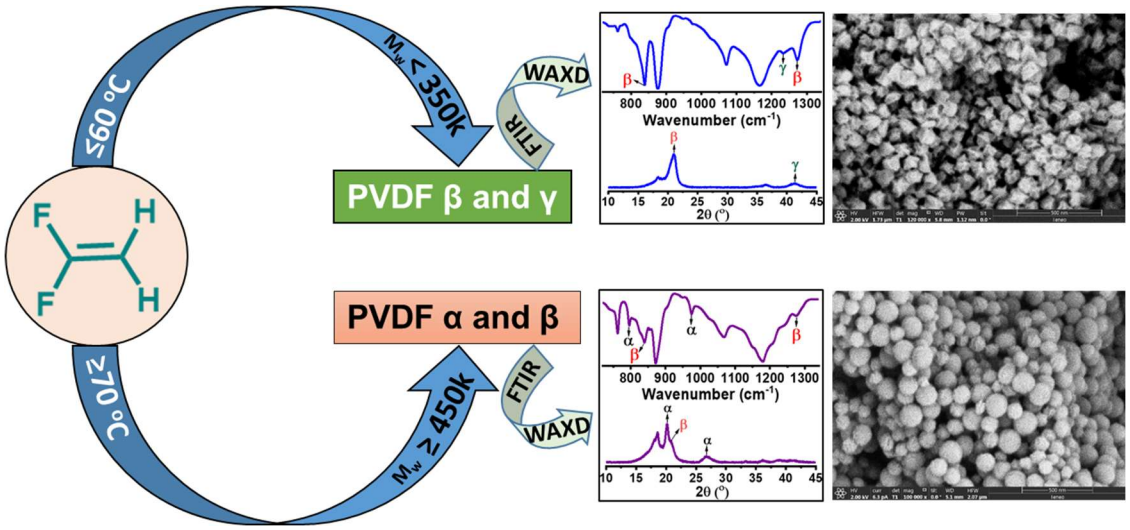

For Table of Contents use only

ABSTRACT: Poly(vinylidene fluoride) (PVDF) received much attention for its electroactive properties arising from β- and γ-crystallographic phases. Up to now, the investigation is reported on post-polymerization processing methods to secure β- and γ-polymorphs, although a deeper understanding of the promotion of β- and γ-phases during the polymerization of vinylidene fluoride (VDF) is scarcely reported. This study scrutinizes the polymerization conditions and demonstrates how polymerization temperatures, times, and molar masses of the "nascent PVDF powder" affect the formation of the crystalline phases (α, β, and γ). It is presented that specific molar masses produced, at various polymerization temperatures, strongly control PVDF polymorphs and play a pivotal role in electroactive phase formation. The molar masses ranging from 100000-350000 $g.mol^{-1}$ and polymerization temperature ≤ 60 °C results into β- and γ-phases, while the molar mass ≥ 450000 $g.mol^{-1}$ at 70 °C polymerization temperature promotes α- and β-phases of the PVDF. Additionally, PVDF chain defects also influence the electroactive phase formations, the lower the chain defects higher is the β-phase content in PVDF. The polymorphs of PVDF homopolymers are identified by Fourier Transform Infrared spectroscopy (FTIR), Raman spectroscopy, and Wide-Angle X-ray Diffraction (WAXD), all these techniques discovered analogous phase identification. Differential Scanning Calorimetry (DSC) and in-situ WAXD experiments are conducted to examine the melting of crystalline phases of PVDF during the heating and cooling process. Thermogravimetric Analysis (TGA) is used to analyze the thermal properties of resultant polymers. Furthermore, the morphology (by Scanning Electron Microscopy, SEM, and Transmission Electron Microscopy, TEM) of the resulting PVDF homopolymers is influenced by the molar masses and different polymorphs of PVDF, a perfect spherical structure is noticed for the higher molar mass and the α-phase of PVDF. Finally, preliminary results on the processing method demonstrate that the nascent PVDF homopolymers can be processed in the solid state,

below their melting temperature, without influencing the polymorph perceived during polymerization. This means that the nascent polymer, having the β-polymorph, retains its crystallographic and conformational structure prior to melting. The transformation from α to β and γ PVDF is accomplished through solid-state processing (compression-rolling-stretching), below the melting temperature of the nascent PVDF homopolymers. Compared to melt and solution processing, the solid-state processing is of advantage as it circumvents work required against entropy to secure oriented chains, and the use of carcinogenic solvents. Moreover, environmental friendly solid-state processing avoids the decomposition of the sample above the melting point that often causes release of the hazardous gases in fluorinated polymers.

INTRODUCTION

PVDF is a specialty polymer that is often used because of its high melting temperature, chemical resistance, and electrical properties in a range of applications.[1-6] PVDF and its copolymers are well-known for their highest dielectric constant and excellent electroactive responses such as piezo-, pyro-, and ferroelectric effects.[7-9] The synthesis of polymeric materials possessing remarkable electroactive properties is more compelling and demanding due to their applicability in energy generation and storage, sensors, actuators, separator and filtration membranes, and smart scaffolds.[10-13] However, the polymer should possess one of its electroactive phases for many of these applications. PVDF is an asymmetric and semi-crystalline polymer and produces five distinct crystalline phases analogous to different chain conformations such as α (trans-gauche-trans-gauche TGTG'), β (all trans-TTT planar zigzag), γ (T3GT3G'), δ (TGTG') and ε (T3GT3G') phases.[8, 14-17] Until now, α-, β-, and γ-phases of PVDF are the most investigated and utilized for applications. Among the three, the α-phase is the most stable, non-polar, and exhibits zero dipole moment. For several applications including sensors and actuators, a strong electric dipole moment of PVDF is

required, which can be achieved with the formation of the transient β- and γ-phases.[18-21] Notwithstanding, β- and γ-phases are the highest electrically active and present excellent electrical properties including piezo, pyro, and ferro. However, their promotion within PVDF material is the most desirable and ongoing challenge.

In this context, several strategies are developed and explored to pursue the electroactive phases of PVDF, mainly focused on the post-polymerization processing procedures such as rate-dependent melt-crystallization[21-28], temperature-dependent solution crystallization[29-31], under high pressure and external electric field[32, 33], film stretching at a different draw ratio[34-37], or the addition of specific fillers[38, 39]. Very recently, Beuermann et al.[40] have shown that the specific molar masses of pure PVDF strongly influence the generation of electroactive crystallographic phases through varying heating/cooling rates. However, this novel approach also deals with post-polymerization treatment. In addition, it is also known that polydispersity (molecular weight distribution) and chain defects/branching significantly affect melt-crystallization behavior.[24, 41-43] So far, electroactive phase formation has been predominantly linked with processing conditions. Notably, polymorphs arising in the nascent PVDF powder (directly obtained from the reactor after polymerization) and their dependence on the polymerization conditions have not been explored so far. Though, the promotion of electroactive phases, during the polymerization of VDF by tuning the polymerization conditions and molar masses could be a straightforward and desirable synthetic approach.

The objective of this work is to investigate how the polymerization conditions and specific molar masses influence the formation of electroactive phases, beyond post-polymerization processing methods. Hence, three different molar masses of the PVDF homopolymers are synthesized by tuning the polymerization conditions. The synthesized PVDF samples are characterized by ^{1}H and

^{19}F NMR spectroscopy to confirm the successful formation of such polymers and to determine the percentage of chain defects. Their different molar masses are accessed by gel permeation chromatography (GPC) while FTIR, Raman, and WAXD techniques are used for the identification of PVDF crystalline phases. SEM and TEM are used to understand the morphology of the polymers. DSC and in-situ WAXD are performed to perceive the melting and crystallization behavior of the PVDF polymorphs. TGA is employed to know the thermal stability of PVDF samples in the state (T_m + 10 ºC) and follow the degradation behavior. Finally, these polymer samples are processed in solid-state (compression-rolling-stretching) below their melting temperature and a 2D WAXD pattern is used to spot orientation after processing.

EXPERIMENTAL SECTION

Materials. Water, purified by Millipore Milli-Q, was used as the polymerization solvent. Potassium persulfate (KPS) (Aldrich, 99%) was recrystallized from water and used as an initiator for the emulsion polymerization of VDF. Pentadecafluorooctanoic acid ammonium salt (APFO) (Aldrich, 98%) was used without any further purification as a surfactant. 1, 1-vinylidene fluoride, VDF (monomer) was received from Apollo Scientific (≥98%) and used as it is.

Characterizations. The ^{1}H and ^{19}F NMR spectra were obtained at 298 K using a Bruker AVQ 500 MHz instrument. Chemical shifts are reported as δ (ppm) values, using either TMS or residual solvent peaks as an internal standard, and coupling constants (J) as Hz values. The molar masses and the molar mass distribution (Đ) of polymers were determined from GPC using an Agilent liquid chromatography system fitted with refractive index (RID) and UV-Vis detectors, using two identical PLgel columns (5 μm, MIXED-C) in connected series with DMF as the mobile phase (1 mL/min). 0.005 M LiBr was added in DMF. The column and flow path were temperatures

controlled at 40 °C. Data analysis was performed using GPC-Addon for ChemStation software from Agilent. DSC measurements were conducted using the TA instruments apparatus. Scans were recorded at a heating and cooling rate of 10 °C·min^{-1} from 30 to 200 ºC. The sample size was about 3-5 mg. FTIR analysis was performed by a Thermo Scientific Nicolet 6700 instrument, equipped with a nitrogen purge and aligned for signal clarity, which was used to collect the data. The instrument was calibrated before sampling against a newly cleaned (acetone) and dried crystal surface. 32 Scans from 4000 to 550 cm^{-1} were recorded for each sample and background. The PVDF samples during the thermal treatment were monitored by in-situ transmission IR, equipped with a Hg-Cd-Te cryo-detector to Harrick controllers. The PVDF powder sample was placed in a quartz IR cell suitable for thermal treatments in a controlled atmosphere. The rate for heating and cooling steps was 10 ºC/min, and the FTIR spectrum at each temperature was captured by averaging 32 scans in mercury cadmium telluride (MCT) mode during the temperature-changing process. Raman measurements of the PVDF samples were carried out using a 532 nm laser with Renishaw micro-Raman spectroscopy system RM2000 (In-Via) at a power of 25 mW. To obtain the spectra, five acquisitions were averaged over 20 repetitions, using an 1800-lines/mm grating. TGA of polymer samples was analyzed under air using a TGA 51 apparatus from TA Instruments at a heating rate of 10 °C min^{-1} from 30 to 700 °C. The sample size varied between 7 and 10 mg. WAXD analysis was conducted with a Bruker D8-advanced (Kα1, λ = 1.5405600 Å) by using Cu Kα radiation. In-situ WAXD experiments were performed in a Xeuss 3.0 system (Xenocs, France) with an X-ray wavelength of 0.154 nm and an operating voltage and current of 50 kV and 0.6 mA, respectively. The system was equipped with a two-dimensional (2D) Eiger2 4 M detector (Dectris, Switzerland) with a resolution of 2162 × 2068 and a pixel size of 75 μm. The distance from the sample to the detector was 100 mm and the exposure time was 300 s for each data. The polymer

powder was wrapped by a Kapton plate and a slice of aluminum foil and fixed in a Linkam HFX350 temperature cell, which was mounted vertically in the transmission mode in a Xeuss 3.0 system. The collected 2D scattering pattern was converted into a 1D intensity curve after subtraction of the background of Kapton and integration operation with XSACT software. 2D WAXD patterns were recorded on a Bruker D8 Eiger diffractometer attached with a Eiger 2R_500 K detector (Cu Kα, λ=1.54 Å). X-ray powers at 40 kV and 40 mA was used for all the measurements. The specimen in the form of nascent powder, disc, or strip was mounted on a sample holder with double-sided tape. The standard sample holder is subsequently placed into the D8 diffractometer in reflection geometry (with the normal of the tape perpendicular to the goniometer and perpendicular to the sample holder). The scan range for the diffraction pattern is from 10° to 60° (2θ) with a step size of 0.01° (2θ). SEM images were taken at FEI Teneo VS microscope (FEI, Hillsboro, OR, USA) which was performed at 2-3 kV and 6.3 pA with an in-lens detector. The working distance was around 5 mm. The polymer powders were dispersed uniformly on stubs with a carbon tab and then coated with 5 nm Iridium. TEM images were collected using an FEI Tecnai Electron Microscope operated at 120 kV in the bright field mode. Samples were prepared by adding a drop of the polymeric solution onto TEM copper carbon-coated grids. The excess of the solution was removed using filter paper and the samples were allowed to dry at room temperature for at least 12h, before observation.

Synthesis of the PVDF homopolymers via Free Radical Emulsion Polymerization. In a typical polymerization, the Parr reactor (100 mL) was filled with APFO surfactant (0.3 wt. %) and KPS as the initiator (0.03 wt. %) dissolved in water (35 mL, 100 wt. %), and nitrogen was purged for 30 min with slow stirring followed by vacuum to remove oxygen from the reactor. The reactor was then evacuated for about 5 min and flushed out three times with VDF at 5 bar. Then, the

monomer (VDF, 12 g, 20 bar) was transferred into the reactor which was then heated gradually up to 60 °C, increased in pressure to 24 bar, and decreased pressure to 15 bar was observed in 14 h. The polymerization was stopped after 15 h and the autoclave cooled to room temperature. After purging the non-reacted monomer, a milky white emulsion was centrifuged for 30 min to obtain a colorless powder settled down in a centrifuge tube. The supernatant liquid was discarded and the product was washed 3 times with excess water. Finally, the product was dried under a vacuum for 24 h at 40 °C. The PVDF homopolymer, as a colorless powder, was characterized by ^{1}H and ^{19}F NMR spectroscopy and GPC.

^{1}H NMR (500 MHz, DMSO-d_6, δ, ppm) (**Figure S1**, Supporting Information): 2.92 (2H, -$CH_2CF_2CH_2CF_2$, normal addition (H-T) of PVDF), 2.26 (2H, $CF_2CH_2CH_2CF_2$, reverse addition (T-T) of PVDF).[44, 45]

^{19}F NMR (500 MHz, DMSO-d_6, δ, ppm) (**Figure S2**, Supporting Information): -91 to -95 (2F, -$CH_2CF_2CH_2CF_2$, normal addition (H-T) of PVDF) and -114 to -116 (2F, $CH_2CF_2CF_2CH_2$, reverse addition (H-H) of PVDF).[44, 45]

RESULTS AND DISCUSSION

The synthesis of PVDF homopolymers is accomplished via free radical emulsion polymerization (**Scheme 1**). A series of VDF polymerizations are carried out at different initiator concentrations, temperatures, pressures, and times (with respect to the initiator half-life time) aiming at various chain lengths of the PVDF homopolymers (**Table 1** and **Table S1**, Supporting Information).

The molar masses of the PVDF homopolymers are tuned by changing polymerization conditions (**Table 1** and **Table S1**, Supporting Information). Three different molar masses of PVDF homopolymers, low (146000 g.mol^{-1}, entry 1, **Table 1**), high (251000 g.mol^{-1}, entry 2, **Table 1**),

and higher (570000 g.mol^{-1}, entry 3, **Table 1**) are synthesized to examine the effect of molar masses on the crystalline forms (α, β, and γ) of PVDF as well as the morphology and thermal behavior of the resulting polymers. The strong shift toward high molar masses is noticed in the GPC chromatograms (**Figure S3**, Supporting Information). It is worth mentioning that the higher molar mass of PVDF (570000 g.mol^{-1}, entry 3, **Table 1**) is achieved at the high polymerization temperature (70 °C) only, and any attempts to synthesize similar or equivalent molar mass at low polymerization temperature (≤ 60 °C) were unsuccessful (entries 1-5, **Table S1**, Supporting Information). Hence, to eliminate the influence of the polymerization temperature on the electroactive phase formation, the low molar mass of PVDF is also synthesized at a high polymerization temperature (70 °C) by varying the initiator concentrations (entry 4, **Table 1**). The polymerization conditions are optimized (initiator concentrations, times, temperatures, and pressure), and the results are depicted in **Table S1** (Supporting Information).

Scheme 1. The synthetic route leading to PVDF homopolymers by free radical emulsion polymerization

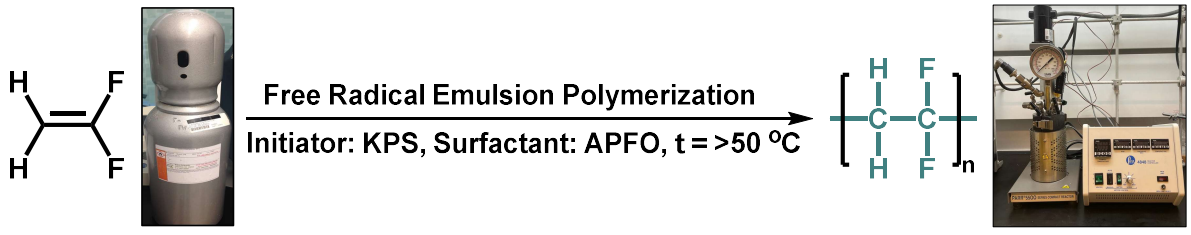

The ^{1}H NMR spectra of PVDF homopolymers show the presence of the characteristic signal at δ = 2.92, and 2.26 ppm corresponding to the normal (head-tail, $-CF_2\underline{CH_2}-CF_2\underline{CH_2}$) and the reverse addition of PVDF (tail-tail, $-CF_2\underline{CH_2}-\underline{CH_2}CF_2$), respectively (**Figure S1**, Supporting

Information). The chain defects (tail to tail) in the PVDF are determined by comparing the integral of the peaks at δ = 2.92 ppm and δ = 2.26 ppm.[44, 45] The ^{19}F NMR spectra are in agreement with the ^{1}H NMR and show the characteristics signals at −91 to −95 ppm, and −114 to −116 ppm due to the normal, and reverse addition of PVDF (head-head, $-CH_2CF_2-CF_2CH_2$ and tail-tail, $-CF_2CH_2-CH_2CF_2$), respectively[44, 45] (**Figure S2**, Supporting Information).

Table 1. Molecular Characterization Data of PVDF homopolymers produced by emulsion polymerization of VDF

Entries	Initiator (Wt. %)	Time (h)	Temp. (°C)	$M_{w,\ GPC}$ ($g.mol^{-1}$)[a]	Đ (GPC)[a]	$T_{m,\ DSC}$ (°C)[b]	$T_{c,\ DSC}$ (°C)[b]	Chain-defect (%)[c]	β-phase content (a.u.)[d]	Polymorphs[e]		
										α	β	γ
1	0.03	15	60	146000	1.53	166 & 172	138	8.25	0.82	-	√	√
2	0.03	33	60	251000	1.76	166 & 172	142	7.40	0.90	-	√	√
3	0.03	9	70	570000	1.75	165 broad	134	10.71	0.52	√	√	-
4	0.18	9	70	176000	1.97	161 & 168	133	8.79	0.73	√	√	√

Polymerization conditions: Solvent: water (35 mL), Pressure: 20 bar, Initiator: Potassium persulfate (KPS), Surfactant: Pentadecafluorooctanoic acid ammonium salt (APFO) (10x to initiator concentrations), Speed: 750 RPM; [a] From GPC (DMF, 40 °C, PS standard, RI detector) (Đ: polydispersity index); [b] From DSC: heating and cooling cycle from 30 to 200 °C, 10 °C/min., (T_m: melting temperature and T_c: crystallization temperature); [c] Determined from ^{1}H NMR using the following formula: [∫2.92 ppm/(∫2.92 ppm + ∫2.26 ppm)] x 100; [d] From FTIR using the following formula[46]: $F(\beta) = A_\beta/(1.3A_\alpha + A_\beta)$; where A_α and A_β are the absorbances in FTIR spectrum corresponding to 763 and 840 cm^{-1} bands, respectively; [e] From FTIR (cm^{-1}): α_{763}, β_{840}, and γ_{1233}.

The polymorphs of PVDF homopolymers as obtained after polymerization (without giving any heat treatment) are examined by FTIR, Raman spectroscopy, and WAXD. The FTIR spectra (**Figure 1A**) clearly indicate the distinct molar masses of PVDF homopolymers strongly influencing the formation of electroactive phases (β and γ). The characteristic bands of each crystalline phase are summarized in **Table 2**. The molar masses of the PVDF homopolymers, ranging from low to high, 100000 to 350000 $g.mol^{-1}$ resulted in β- and γ-phases (entries 1-2, **Table 1**, **Figure 1A(a)** and **1A(b)**, and entries 1-5, **Table S1**, **Figure S4a-e** in Supporting Information). Whereas, the higher molar masses (450000 to 600000 $g.mol^{-1}$) exhibit α- and β-phases (entry 3,

Table 1, **Figure 1A(c)**, and entries 6-8, **Table S1**, **Figure S4f-h** in Supporting Information). As evident from the visual inspection of the FTIR peak at 1233 cm^{-1}, it can be concluded that the β-phase content increases marginally with increasing molar mass of PVDF, whereas the γ-phase content is high in the low molar masses of PVDF. In the case of the higher molar masses of PVDF samples, the α-phase is more dominating. From the above results, it is clear that in the low, high, and higher molar masses of the nascent PVDF observed β and γ (more γ), β and γ (more β), and α and β (more α) phases, respectively. However, it should be noted that the polymerization temperature is non-identical in the synthetic procedures. In order to understand the role of polymerization temperature on the electroactive phase formation, the low molar mass PVDF is synthesized at a high temperature (70 ^{o}C). Interestingly, the low molar mass PVDF obtained at 70 ^{o}C (entry 4, **Table 1**) generates all three crystalline phases (α, β, and γ), among the three, β-phase content was the highest (**Figure 1A (d)**) but still low when compared with the low molar mass of PVDF synthesized at 60 ^{o}C (entry 1, **Figure 1A(a)**). Moreover, to further extend our understanding of the polymerization temperature dependence on the electroactive phase formation, the low molar mass of PVDF is synthesized at the lower polymerization temperature (50 ^{o}C). Analogous to the low polymerization temperature, 60 ^{o}C (entry 1, **Table 1**), β and γ crystalline phases are formed at the chosen polymerization temperature of 50 ^{o}C (entry 5, **Table S1**, and **Figure S4e**, Supporting Information). These results clearly indicate that the combination of specific molar masses (low and high, 100000 – 350000 $g.mol^{-1}$) and the polymerization temperature (≤60 ^{o}C) is the key to the formation of the electroactive phases (β and γ) in PVDF. Raman spectroscopy complements information obtained by FTIR, from **Figure 1B** it is observed that entry 3 has a very high content of α phase (Raman Band at 795 cm^{-1}), while entry 1 and entry 2 have a high content of β-phase (Raman Band 839 cm^{-1}).[47-51] Though Raman spectroscopy cannot identify the presence of the γ

phase, due to the overlap of the peak at 839 cm^{-1} with the β-phase[51], FTIR data in combination with WAXD (**Figure 3**) does suggest its presence in entry 1 and the entry 2. The information on the three polymorphs and their association with the respective vibrational bands and the diffraction planes is summarized in **Table 2**.

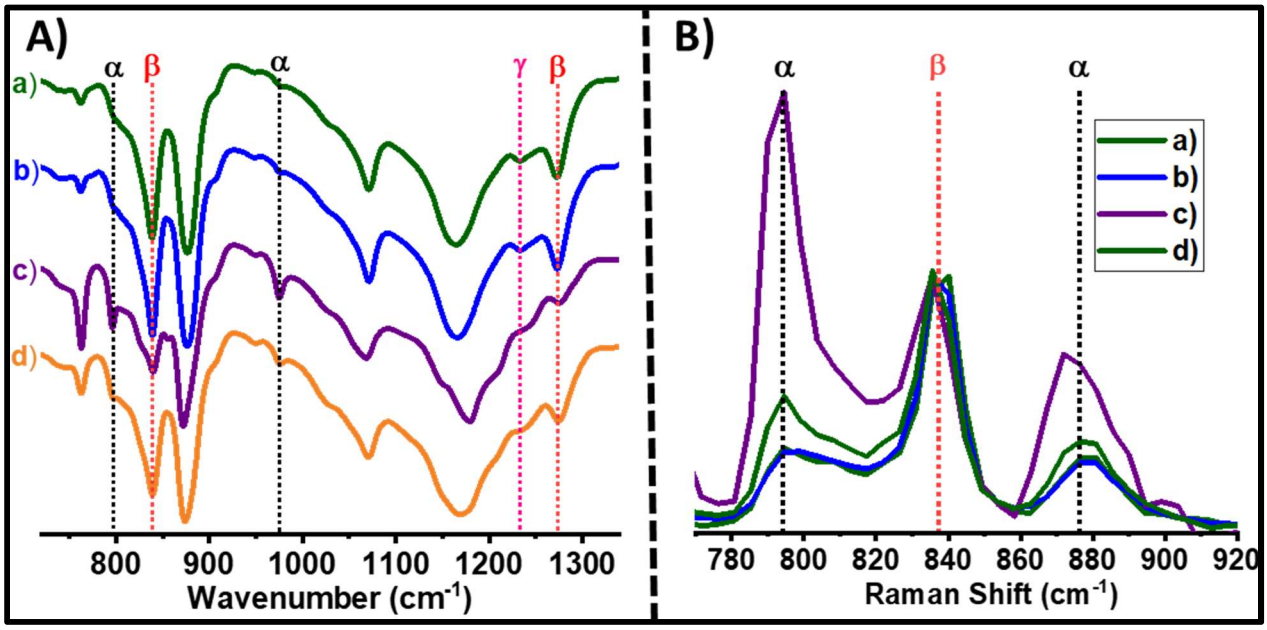

Figure 1. A) FTIR spectra and B) Raman spectra (normalized β-phase at 839 cm^{-1}) of various crystalline phases of nascent PVDF homopolymers recorded at room temperature: a) M_w: 146000 (entry 1, Table 1), b) M_w: 251000 (entry 2, Table 1), c) M_w: 570000 (entry 3, Table 1), and d) M_w: 176000 (entry 4, Table 1).

Table 2. Characteristics of FTIR and Raman bands, WAXD diffraction crystal plane, and apparent DSC temperature range of α-, β-, and γ-phases of PVDF[8, 51]

Crystal	FTIR	Raman	WAXD		DSC
phases	Wavenumber (cm^{-1})	Wavenumber (cm^{-1})	*2θ* (°)	Crystal plane	(°C)
α	614		17.90°	(100)	
	763		18.55°	(020)	

	795	796	20.14°	(110)	165-172
	976		26.74°	(021)	
β	840	839	20.90°	(110/200)	
	1278				165-172
γ	833		18.32°	(020)	
	840	839	20.02°	(110)	178-182
	1233		41.34°	(140)	

The influence of PVDF chain defects on the electroactive phase formation is also investigated. In principle, the lower the chain defects (head-head and tail-tail), the higher is the normal addition of the PVDF chain (head-tail), which is the most favorable chain conformation for the synthesis of electroactive phases, exclusively the β-crystalline phase (all trans-TTT, planar zigzag).[9,52] The findings in this work confirm that lower chain defects of the PVDF chain (tail-tail) produce more β-phase content (entry 2, **Table 1**, and **Figure 2**). The superior head-tail addition of the PVDF chain resembles the PVDF β-phase having all trans planar zigzag chain structure.

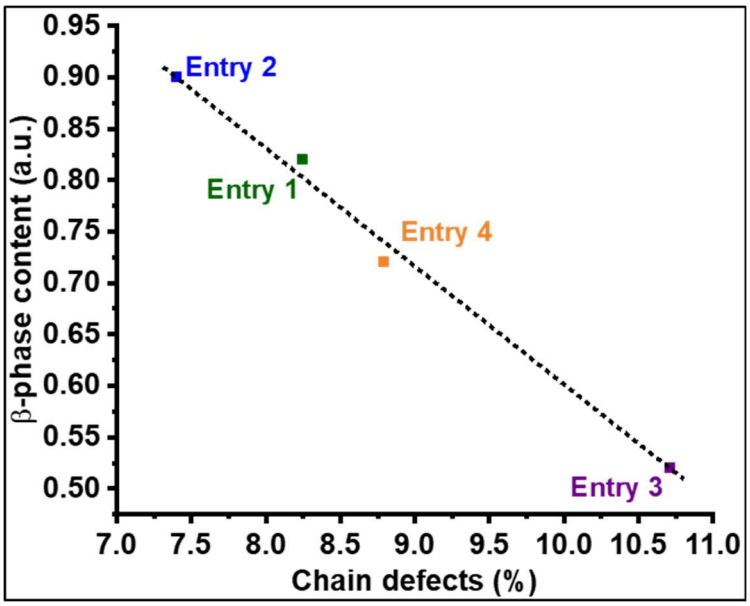

Figure 2. Chain defects vs. β-phase content in the PVDF homopolymers (entries 1-4, Table 1). From the figure, it is apparent that the lower the chain defect more prominent is the β-phase (Entry

2), whereas the phase that can include the most defects is the α-phase (Entry 3). The mixture of the two phases is anticipated in Entry 1 and Entry 4.

The polymorphs of the PVDF homopolymers, as obtained on crystallization during polymerization, are further investigated by WAXD. The diffraction angle and the associated crystalline planes, to the polymorphs, are summarized in **Table 2**. The conclusions drawn over the polymorphs of PVDF are in agreement with the crystallographic variations observed by WAXD (**Figure 3** and **Figure S5**, Supporting Information) and conformational changes by FTIR and Raman spectroscopy (**Figure 1**).[8, 53] It is widely acknowledged that the FTIR and Raman spectroscopy alone cannot identify β or the γ-phase due to the presence of the identical bands at 840 cm^{-1} (FTIR) and 839 cm^{-1} (Raman) for both polymorphs. Although the vibrational mode in the presence of the β-phase, is stronger at 840 cm^{-1} (FTIR) and 839 cm^{-1} (Raman), in the presence of the γ-phase an additional band as a weak shoulder appears at 833 cm^{-1} in FTIR. The weak shoulder band is supplemented by a distinct FTIR absorption band at 1233 cm^{-1} attributed to the γ-phase (**Figure 1Aa** and **1Ab**). In WAXD, because of the overlapping of the crystal diffraction planes (020) and (110), the polymorphs α and γ-phases, cannot be distinguished easily. The exclusivity of the diffraction peak associated with the crystal plane (021) for the α-phase (**Figures 3c** and **d**), and the crystal plane (140) for the γ -phase (**Figures 3a** and **b),** allows making the distinction between the two phases. The presence of the β-phase is identified by a well-defined diffraction peak at $2\theta = 20.3^{o}$ associated with the overlapping of the (110) and (200) diffraction planes of the β-phase.[8, 54-57] The complementary FTIR, Raman, and WAXD techniques allow the exact identification and quantification of the PVDF crystalline phases.

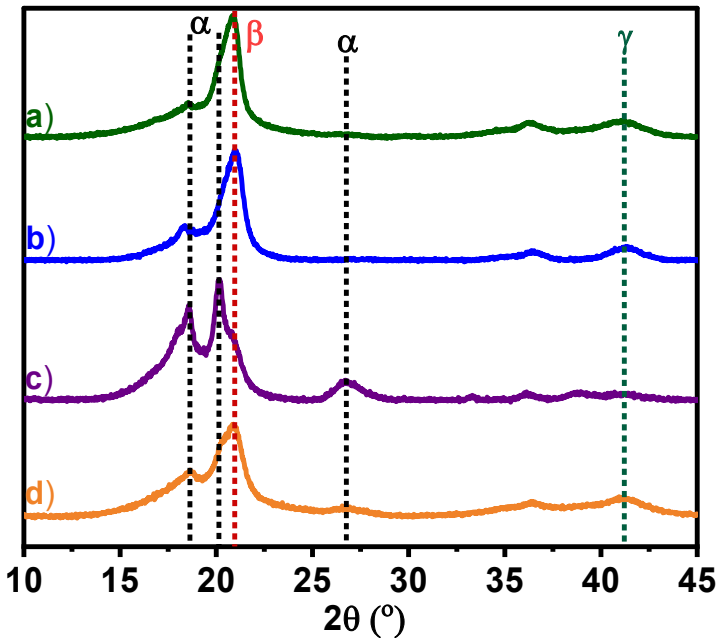

Figure 3. WAXD patterns of nascent PVDF homopolymers at room temperature: a) M_w: 146000 (entry 1, Table 1), b) M_w: 251000 (entry 2, Table 1), c) M_w: 570000 (entry 3, Table 1), and d) M_w: 176000 (entry 4, Table 1).

According to the information available in the literature, DSC was also used as a complementary technique for the identification of the PVDF polymorphs. However, the exact melting temperatures of different crystalline phases of PVDF are debatable.[8, 40, 58, 59] Disagreement arises because different melting peaks of PVDF appear in the DSC thermograms that are attributed to: a) different crystalline phases, b) characteristics of the morphology (chain defects, size, etc.), and c) melting-recrystallization phenomenon. According to several reports, the expected melting temperature of the α-phase is 172 °C while a few reports also suggest its melting temperature at 167 °C.[8] Interestingly, the β-phase represents the closer melting temperature of the α-phase[8], whereas, the γ-phase melting temperature is comparatively higher than the melting temperature of the α- and β-phase.[8, 40] Therefore, DSC alone cannot specify an exact melting temperature for the different

crystalline phases, but a temperature range. In **Figure 4**, the DSC thermograms include the 1st heating and cooling run of the nascent samples and it is apparent that both entry 1 and entry 2 show two melting peaks at relatively high temperatures (166 and 172 ºC, entries 1 and 2, **Table 1**, **Figure 4a** and **4b**) compared to entry 3 (165 ºC, entry 3, **Table 1**, **Figure 4c**). However, it should be noted that the present investigation deals with the nascent PVDF system containing a mixture of the polymorphs, whereas the accepted melting temperature range for PVDF-crystallites in the existing literature associated with the post-polymerization treatments that produce exclusively pure phases. Notwithstanding, DSC features are not only dependent on the crystalline phase, but are also affected by crystalline defects which are particularly enhanced by the chain defects, molecular weights, and polymerization conditions. Considering these assumptions, we have not used the DSC technique to distinguish crystalline phases of PVDF and choose to rely on FTIR, Raman, and WAXD techniques to differentiate polymorphs of PVDF.

The thermal stability and melting behavior of near defect-free piezoelectric β-phase (**Figure 2**) is followed by in-situ WAXD experiments through heating or cooling of the nascent sample (entry 2, **Table 1**). **Figure S7** in supporting information represents the full WAXD pattern of entry 2 while heating the nascent sample to 200 ºC and subsequently cooling it at room temperature, however, the selected heating and cooling WAXD pattern is shown in **Figures 5a and b** for better and clearer understanding. It is observed that till 160 ºC all phases present in the nascent sample are preserved during the heating process (**Figure S7a**, and **Figure 5a**). As temperature further increases until 166 ºC, the β-phase dramatically decreases and the appearance of a new tiny peak, α-phase, is observed (**Figure 5a**). At 168 ºC, the β-phase completely disappears (melts) and a tiny fraction of the α-phase is noticed (**Figure 5a**). However, no crystalline fragments survive above 168 °C, a temperature above the end melting temperature of the PVDF homopolymer (entry 2,

Table 1) measured by DSC (**Figure 4b**). By combining with in-situ WAXD-heating (**Figure 5a**) and DSC-heating results (**Figure 4b**), the peak at 166 ºC could be assigned to the melting peak of β-phase crystal, while the tiny peak around 169 ºC associated with α-phase. This is typical for the normal melt-recrystallization behavior of PVDF. Furthermore, **Figure S8** in supporting information represents the subtraction/separation of the amorphous and crystalline region in the 168 ºC WAXD curve and confirms the presence of the α-phase before complete melting occurs. The resultant crystallization from the melt starts from 150 ºC (also confirmed by DSC-cooling from melt (**Figure 4b**)) and suggests the dominance of the α-phase (**Figure 5b and Figure S7b**). However, in the region of 170-200 ºC, the polymer sample stays in the liquid state.

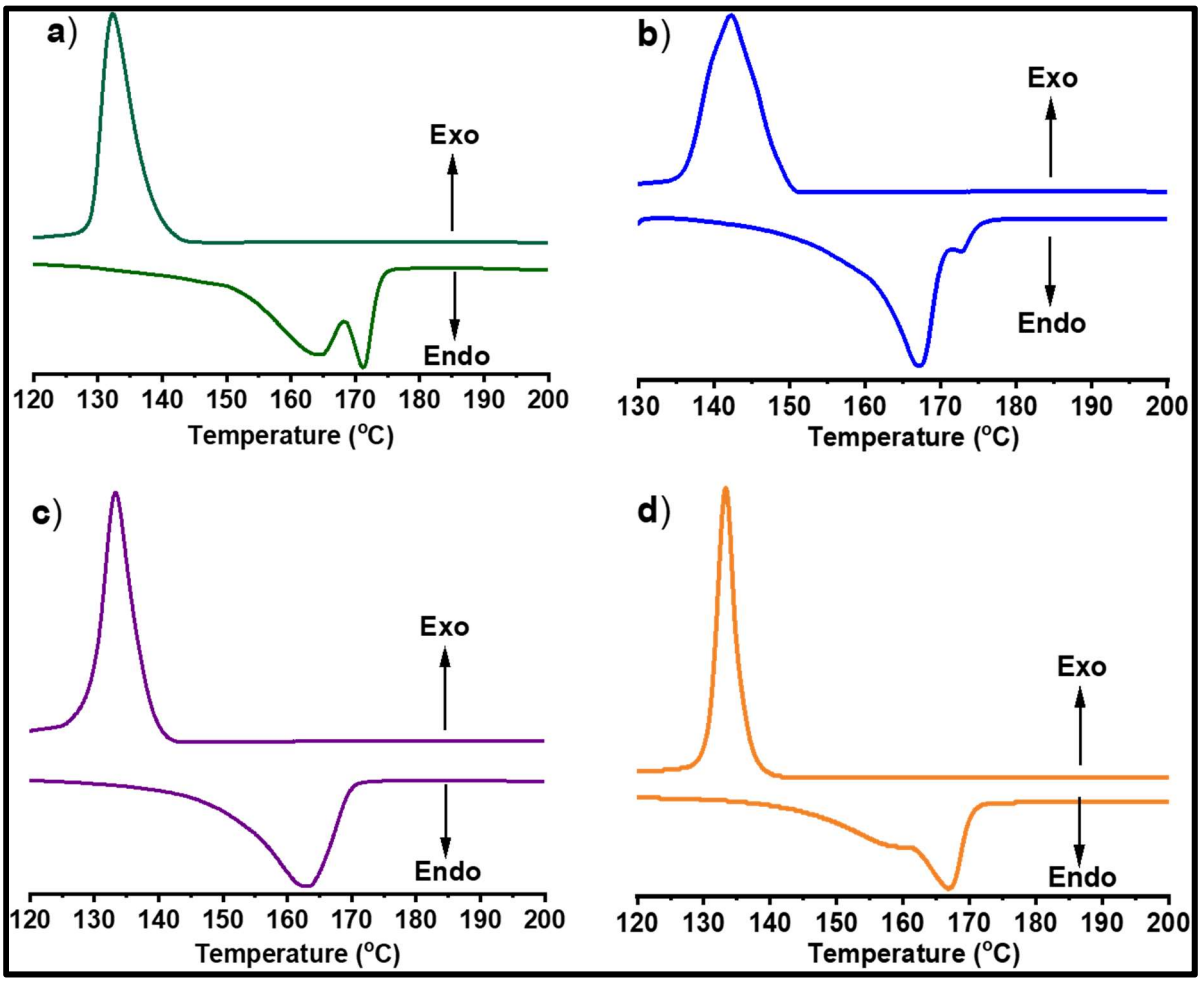

Figure 4. DSC thermograms of nascent PVDF homopolymers (1st heating and cooling): a) M_w: 146000 (entry 1, Table 1), b) M_w: 251000 (entry 2, Table 1), c) M_w: 570000 (entry 3, Table 1), and d) M_w: 176000 (entry 4, Table 1) at 10 °C/min.

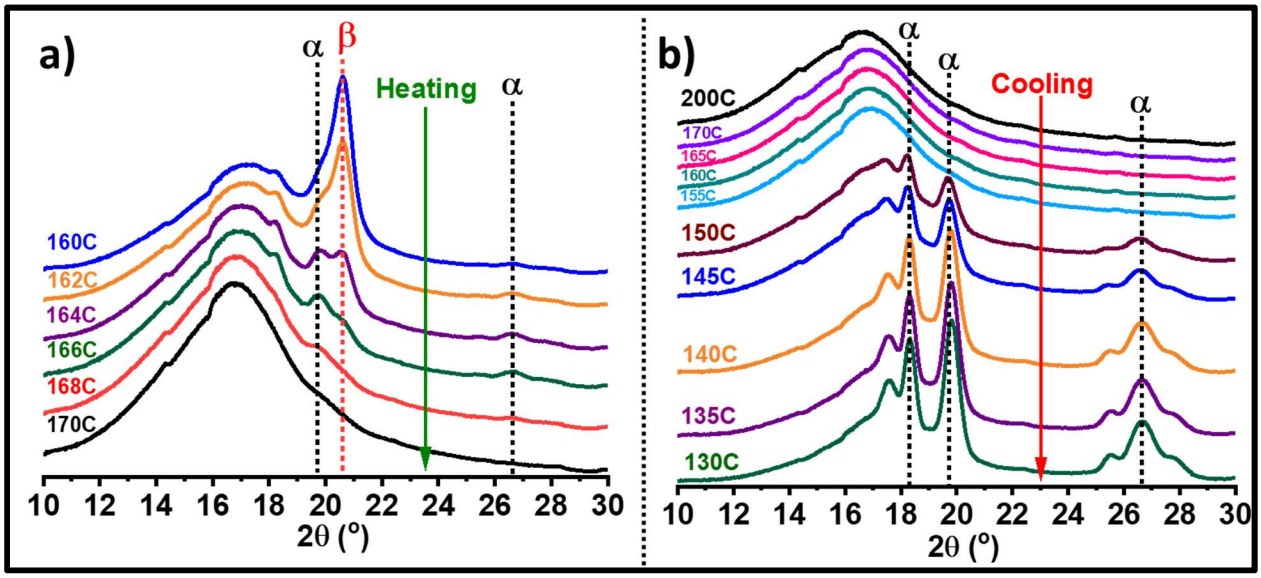

Figure 5. In-situ WAXD pattern of nascent PVDF homopolymer (entry 2, Table 1): a) during heating, and b) subsequently cooling.

Furthermore, the melting behavior of slightly high-defected piezoelectric β-phase (**Figure 2**) is also monitored by in-situ WAXD through heating of the nascent sample (entry 1, **Table 1**) from room temperature to 200 °C and subsequent cooling to room temperature (**Figure S9**, Supporting Information). In contrast to the entry 2 sample, until 170 °C, all phases present in the nascent sample are preserved during the heating process (**Figure S9a**). As temperature further increases until 176 °C, the β-phase dramatically decreases and completely disappears at 178 °C, and a new peak is noticed as the α-phase. Interestingly, crystalline fragments belonging to the α-phase survive above 178 °C (**Figure S9a**, Supporting Information) and remain until 200 °C as confirmed by the subtraction/separation of the amorphous and crystalline region in 200 °C WAXD curve (**Figure S10**, Supporting Information). To extend further understanding, DSC is performed at a slow

ramping rate (1 ºC/min) (**Figure S11**, Supporting Information) to be beneficial for the recrystallization and better resolution of PVDF crystalline melting peaks. The small discrepancy in the temperature between WAXD-heating (**Figure S9a**) and DSC-heating results (**Figure S11**, Supporting Information) is observed due to the different heat transfer lags in the variable temperature control units of the employed characterization techniques. The contact heat transfer between the sample and the hot plate applied in DSC is more effective than the hot stage attached to the WAXD. Moreover, the different enhancement of the peak intensity under cross-polarization due to the different sample density may also be considered as a possible reason. The entry 2 sample is observed as low density and low peak intensity as compared to the entry 2 sample. Hence, the low density leads to low heat transfer and results in temperature variation.

An in-situ FTIR experiment of the PVDF sample (entry 1, **Table 1**) was recorded during the heating process from room temperature to 150 ºC and the subsequent cooling to room temperature at the rate of 10 ºC/min (**Figure S12,** Supporting Information). The quartz IR cell containing a harrick disk, suitable for thermal treatments in-situ FTIR, damages upon the heating of the polymer sample above their melting temperature. Due to this limitation, the PVDF sample is heated below their melting temperature. It is observed that till 150 ºC all phases present in the nascent sample are preserved during the heating and the cooling cycle (**Figure S12,** Supporting Information).

The in-situ WAXD and FTIR results in **Figures 5, S7, S9, and S12** are further strengthened by following the resultant phase after giving the samples thermal treatment in DSC (**Figure S13**, Supporting Information), this is also to avoid any thermal lag that may arise during measurements in FTIR and WAXD. **Figures 6** and **7** show the resultant spectroscopic and crystallographic changes recorded at room temperature after giving the thermal treatment in DSC (**Figure S13**, Supporting Information). The sample (entries 1 and 2, **Table 1**) is prepared in DSC by heating the

nascent sample from room temperature to the chosen temperatures of 150 ºC (**Figure S13a**), 160 ºC (**Figure S13b**), 170 ºC (**Figure S13c**), 180 ºC (**Figure S13d**), 190 ºC (**Figure S13e**) and 200 ºC (**Figure S13f)** and isothermal annealing for 1 min at the chosen temperature and subsequent cooling to room temperature. The samples thus obtained, at room temperature, are investigated by FTIR (**Figure 6**) and WAXD (**Figure 7**). From **Figures 6** and **7**, it is apparent that the nascent powder has the majority of the β-phase. However, on annealing at the chosen high temperatures, the content of the β-phase remains the same till 160 ºC. With the onset of melting, as recorded by DSC (**Figure S13**), on annealing at 170 ºC and beyond the diffraction peak and conformational modes associated with the β-phase decrease while the α-phase increases. We attribute the strengthening of the α-phase to the crystallization of the polymer on cooling from the partial molten state as apparent from DSC (**Figure S13**). These findings are in agreement with the in-situ WAXD and FTIR measurements that conclusively demonstrate the robustness of the β-phase prior to melting. The retention of the β-phase at higher temperatures is an important observation that can be exploited if the polymer can be shaped below the melting point.

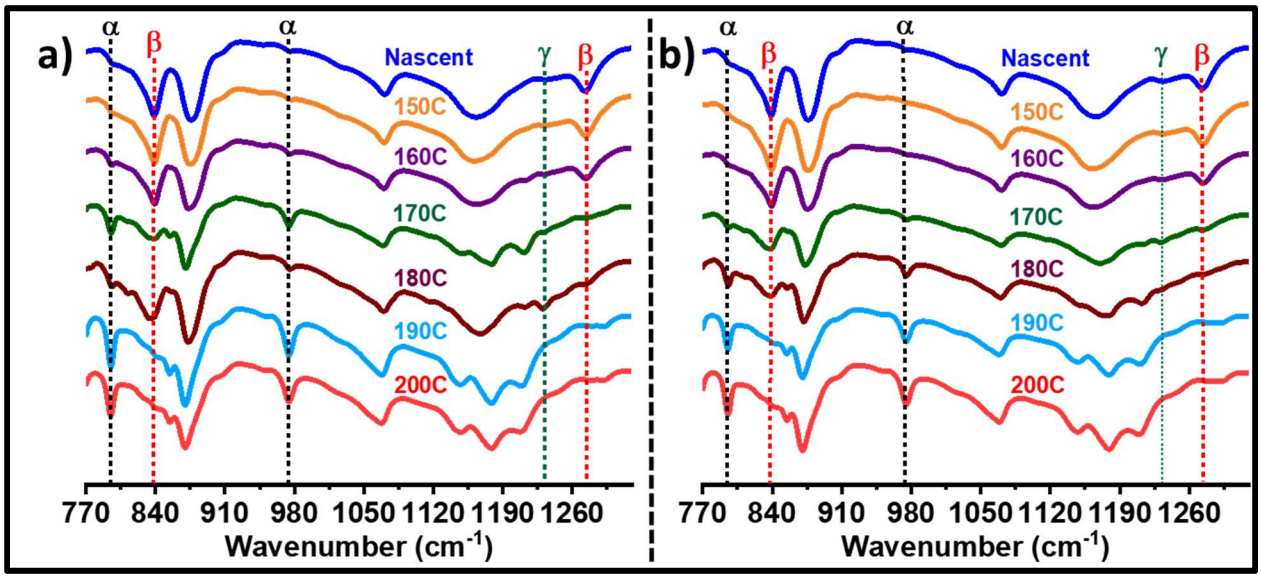

Figure 6. FTIR spectra of PVDF homopolymer: a) entry 1, Table 1 and b) entry 2, Table 1 recorded at room temperature while the sample was prepared using DSC by heating the nascent polymer to 150, 160, 170, 180, 190, and 200 ºC and subsequently cooling to room temperature (Figure S13).

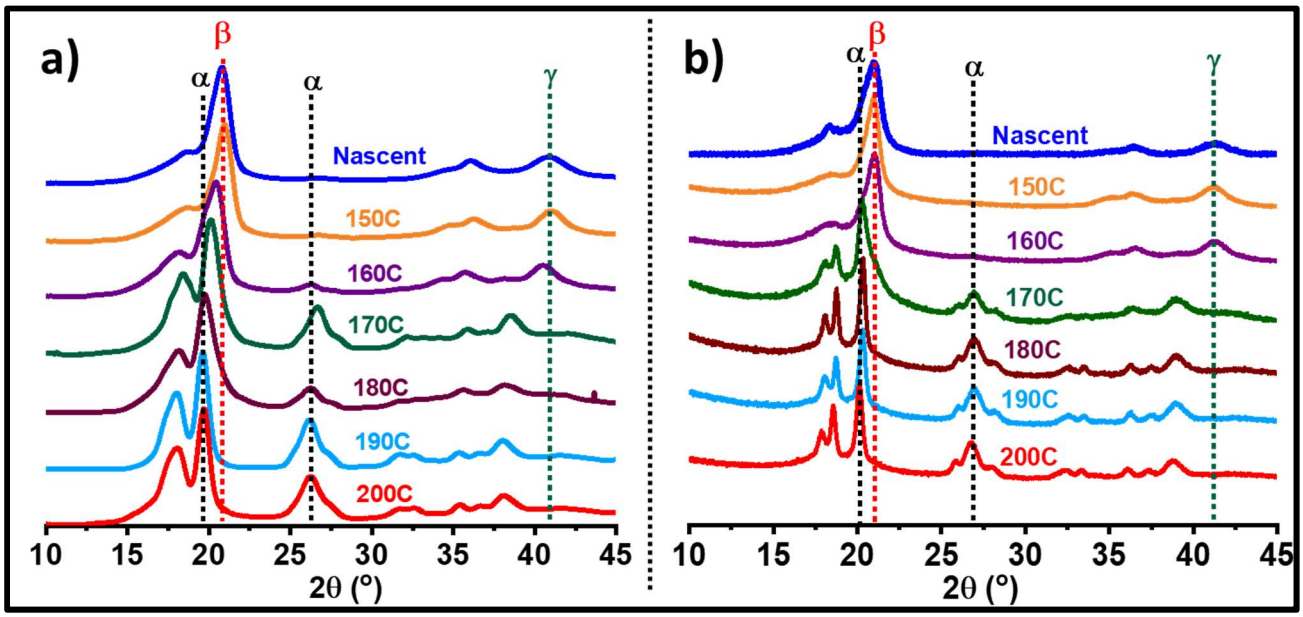

Figure 7. WAXD pattern of PVDF homopolymer: a) entry 1, Table 1 and b) entry 2, Table 1 recorded at room temperature while the samples were prepared using DSC by heating the nascent polymer to 150, 160, 170, 180, 190, and 200 ºC and subsequently cooling to room temperature (Figure S13).

The morphology of the PVDF homopolymers (entries 1-4, **Table 1**, and entries 1-8, **Table S1**, Supporting Information) is investigated using SEM. The specific molar masses and various crystalline phases of PVDF have a profound influence on the morphology, especially the shape and size of the nascent particles (**Figure 8**, and **Figure S14**, Supporting Information).[60, 61] It should be noted that the higher α-phase content (more chain defected) is only obtained at higher molar masses of the PVDF. Morphology grows into the perfect spherical structure as the molar masses

of the PVDF increase (α-phase) (**Figure 8a-c**, and **Figure S14**, Supporting Information). Indeed, the adopted polymerization conditions are found to have implications on the resultant morphology that SEM in **Figure 8** and the supplementary section demonstrates. Variation in the morphology, with increasing temperature and molecular weight, changing from faceted crystals (predominantly β-phase) to symmetric spherical structure (α-phase) (**Figure 8a, 7b, 7c**) is indicative of the increasing chain defects – an observation equivalent to changes in the faceted crystals of long alkanes reported by Organ[62] and Ungar.[63] Additionally, particle size also increases as the molar mass of PVDF homopolymers increases. To gain further insights into molar mass-dependent morphology, TEM images are collected for entries 1-4 in **Table 1** (**Figure S15**, Supporting Information) and are in general agreement with the SEM data. An excellent spherical structure is observed with the higher molar mass and α-phase content of PVDF homopolymers.

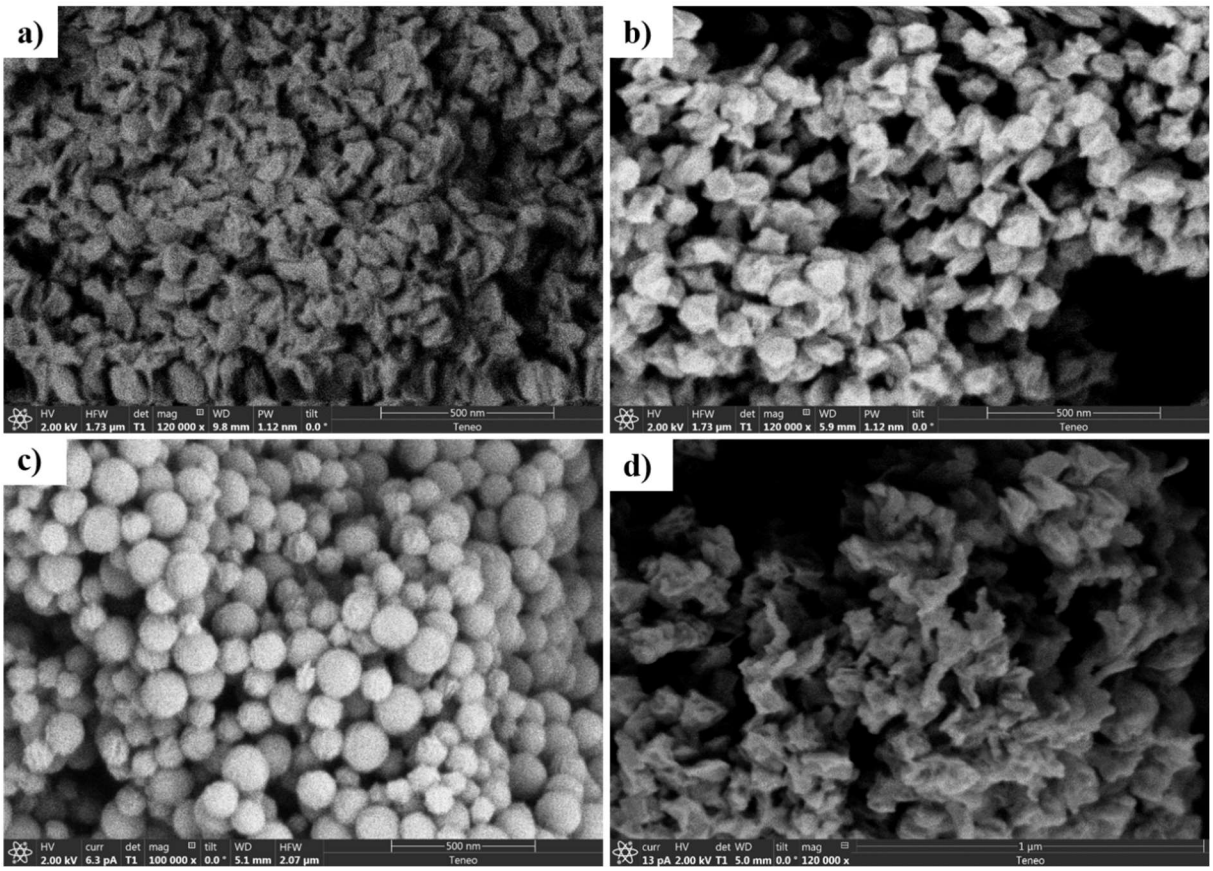

Figure 8. SEM images of PVDF homopolymers: a) M_w: 146000 (entry 1, Table 1, β-phase), b) M_w: 251000 (entry 2, Table 1, β-phase), c) M_w: 570000 (entry 3, Table 1, α -phase), and d) M_w: 176000 (entry 4, Table 1, β-phase/ α -phase).

Finally, the thermal stability of these polymers is investigated by TGA under air (**Figure S16**, Supporting Information).[64] The thermal stability increases with the molar mass of the polymers; the higher the molar mass, the higher is the thermal stability reaching up to 450 ºC (**Figure S16**, Supporting Information). The thermal stability is also explored in the molten state of these polymers (T_m + 10 ºC) for 12 hours of annealing. It is found that the low molar masses of PVDF lost approximately 2% of weight, while the higher molar masses of PVDF lost less than 1% of the weight (**Figure S17**, Supporting Information).

Until now, the literature survey revealed the formation of the most promising electroactive phases in PVDF by post-polymerization processing methods.[21-40] However, in the results and discussion, we demonstrate how the nascent PVDF powder (entries 1-2, **Table 1**, and entries 1-5, **Table S1**, Supporting Information) directly produces electroactive phases (β and γ) without any processing steps. In order to use such materials in real-world applications[65], it is important to preserve the "nascent" behavior of the PVDF after its processing. The processing conditions of PVDF, especially in the form of film, have been investigated by several groups to analyze their temperature limits that can be used for practical application. [66-69] In previous studies as well as in the current findings, it has been found that the β-phase is stable below the melting temperature of PVDF. [66-69] However, it is important to process such material below its melting temperature to preserve the β-phase. As a proof of concept, in an exploratory trial, the highest β-phase content of the PVDF (entry 2, **Table 1**) is fabricated (compressed) into the form of a disc (thickness = 0.5 mm) using a Collin hot press below the melting temperature of the PVDF (130 ºC) (**Figure 9**).

The compressed disc is partially transparent (due to below-melting sintering) but resilient. The FTIR and WAXD measurements of the compressed PVDF disc are well-matched with the nascent PVDF powder (**Figure 9**). This performance implies that the nascent behavior is thoroughly maintained without compromising the most interesting electroactive properties (β and γ) after processing. This feature is particularly important to process such materials in a solid state (below their melting temperature) to avoid the possibility of degradation or release of hazardous gas[70, 71], where the nascent polymer without melting, as received from the reactor, can be molded into desired shapes while retaining the polymorph perceived during polymerization.

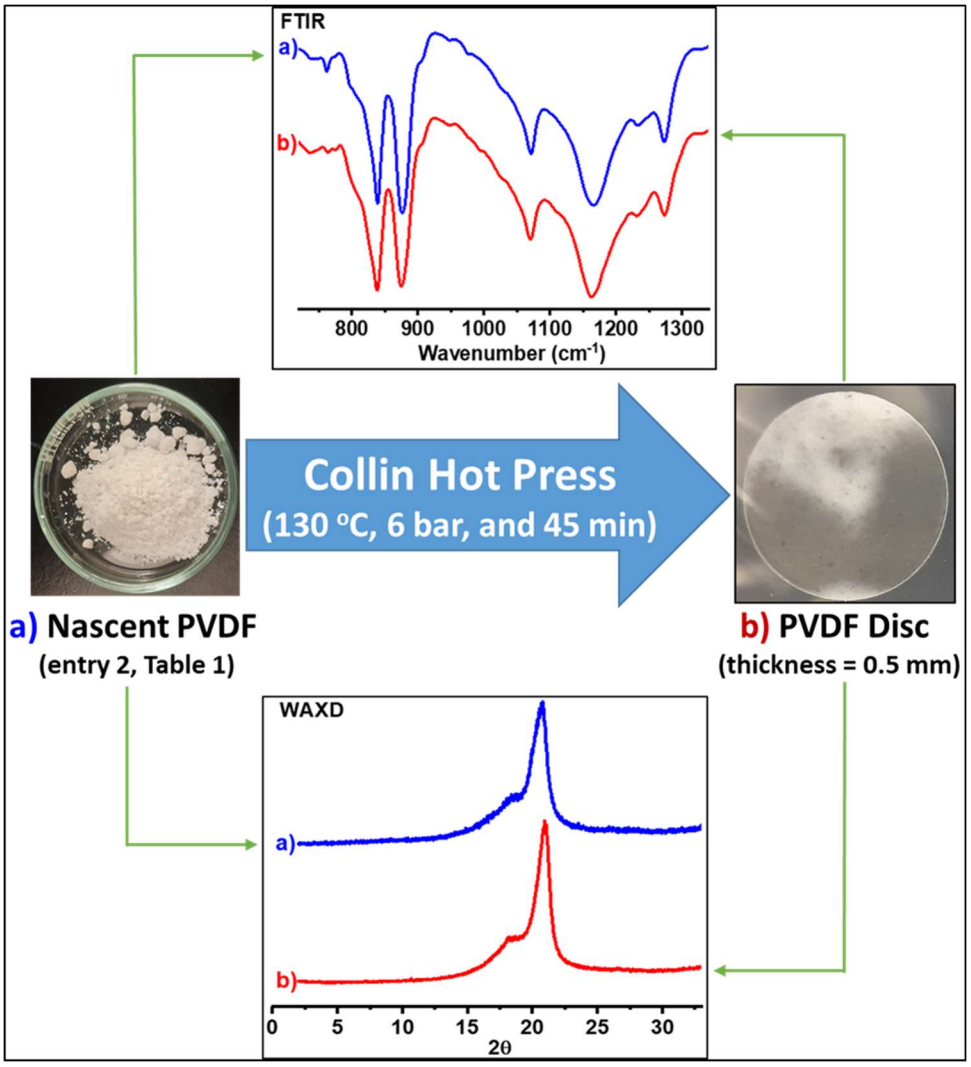

Figure 9. Compaction of PVDF nascent powder into the disc using Collin hot press and characterized by FTIR and WAXD before and after compression: a) nascent PVDF powder (entry 2, Table 1, β -phase), and b) PVDF disc (after compression in β -phase). The compression in the hot press is done at 130 ºC and a pressure of 6 bars.

Furthermore, we also validate the phase transformation from α to β and γ PVDF over the rolling and stretching process using the highest α-phase content PVDF (entry 3, **Table 1**). Up to now, the analogous transformation was achieved through the rolling-stretching/drawing process by making a polymer film either by solvent casting or melt processing techniques.[34-37] In the present investigation, a polymer strip is made by Collin hot press, compression (rectangular mold) below the melting temperature of the PVDF (130 ºC, thickness = 0.25 mm and length = 5 cm), and subsequently rolled (over rolling mills, thickness = 0.1 mm and length = 13 cm) and partially stretching (over Kofler bench, length = 21). The WAXD patterns of the PVDF sample (entry 3, **Table 1**) are shown in **Figure 10**. The 1D diffraction pattern of the nascent PVDF powder and the same compressed strip showed identical intensities which correspond to α (major) and β (minor) phases (**Figure 10a**). In addition, a 2D diffraction pattern confirms no orientation in nascent and compressed samples (**Figure 10b**). Again, these outcomes suggest the control of "nascent" behavior after the compression of nascent PVDF powder below its melting temperature. However, upon rolling and partially stretching, the disappearance of the α-phase and the formation of new β and γ-phases are noticed in the 1D diffraction pattern (**Figure 10a**). Besides, a visible orientation is also observed in a 2D diffraction pattern (**Figure 10b**) consequent to rolled and partially stretched samples. These preliminary attempts for processing suggest that the PVDF samples can be solid-state processed below their melting temperature, via an environmental friendly route.

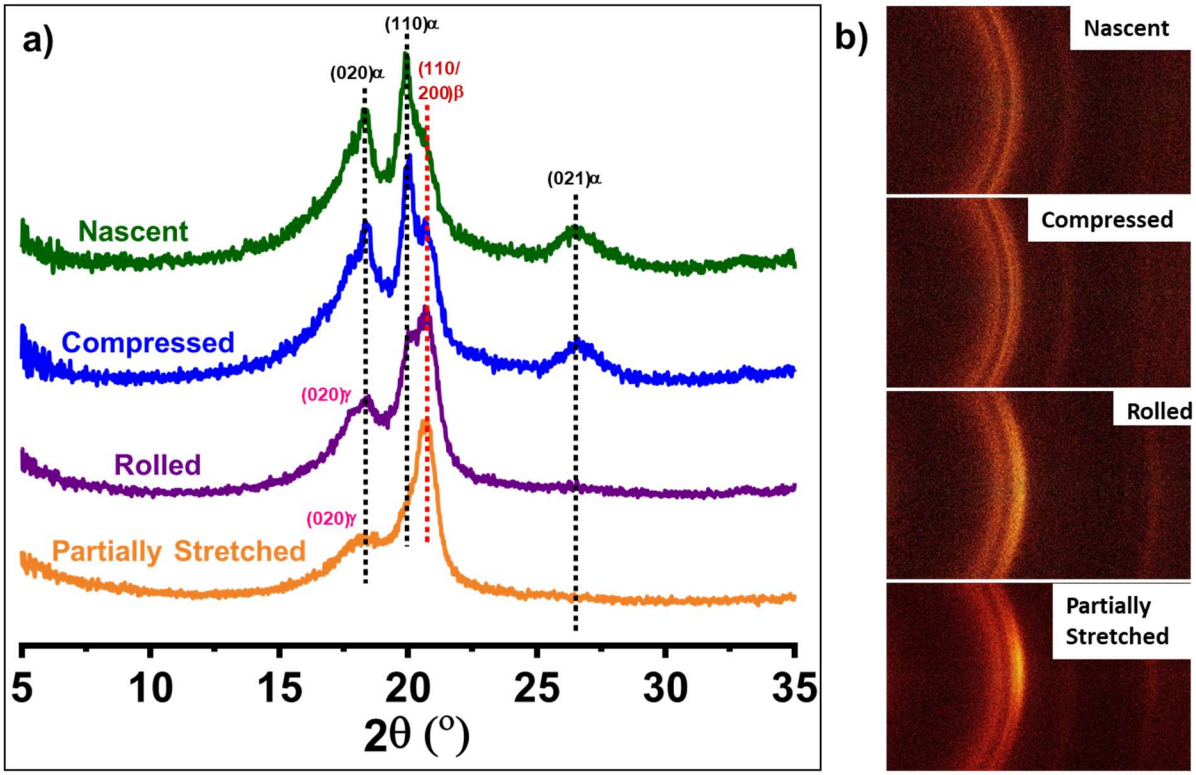

Figure 10. a) WAXD patterns of nascent PVDF powder (entry 3, **Table 1,** α -phase) (green), compressed strip (blue, α -phase), rolled sample (purple, predominantly β -phase), and partially stretched sample (orange, β -phase) recorded in reflection mode using a one dimension detector where the samples were rotated around their axis while recording the diffraction, **b)** WAXD 2D diffraction patterns of the same samples, recorded in the transmission mode using a 2D detector.

CONCLUSIONS

A series of PVDF homopolymers are synthesized via free radical emulsion polymerization. The molar masses and their synthesis temperature strongly influence the polymorphs of PVDF homopolymers. The combination of specific molar masses, 100000-350000 $g.mol^{-1}$, and polymerization temperature ($\leq 60^{o}C$) enables the formation of the most interesting electroactive phases (β and γ). The phase identification of these polymers is supported by FTIR, Raman, and

WAXD. All these techniques unanimously identify the resultant phase perceived during polymerization and processing. DSC showed higher melting temperature for the mixture of β- and γ-phase as compared to the α- and β-phase mixture. In-situ WAXD demonstrates the thermal stability and melting behavior of PVDF crystallites. In addition, chain defects of PVDF homopolymers also had an impact on the formation of the electroactive phases: the lower the chain defects, the higher is the β-phase content in PVDF. The morphology of these polymers is observed by SEM and TEM and is found to be strongly influenced by the molar masses and polymorphs of PVDF. From SEM it is apparent that the faceted morphology of the β -phase changes to spherical with increasing chain defects and appearance of the α -phase. As molar masses of PVDF homopolymers increase (α-phase), a perfectly spherical shape morphology is developed, and the size of the spherical particles increases. TGA validates the superior thermal stability of these polymers that tend to increase with increasing molar mass. The nascent PVDF samples having the highest β- and γ-phase content are found to be stable even after solid-state processing below melting temperature. Additionally, the transformation from α to β and γ PVDF is also achieved during solid-state processing (compression-rolling-stretching) below their melting temperature.

The formation of the most beneficiary electroactive properties (β- and γ-phase) of PVDF homopolymers, through the nascent structure of polymer (without additional treatment), is a particularly fascinating and desirable approach for numerous applications including sensors, actuators, and energy harvesting.[65, 72] Finally, this simple and robust synthetic approach opens a new perspective toward the development of electroactive properties. Efforts to gain additional information about their mechanical stretching, melt-crystallization, and annealing behavior, and measurements of ferroelectric properties and piezoelectric response are currently underway in our

laboratory. Furthermore, attention will be devoted to the development and use of non-fluorinated surfactants for emulsion polymerization.[73]

ASSOCIATED CONTENT

Supporting Information.

This material is available free of charge via the Internet at http://pubs.acs.org.

Table- Optimized polymerization conditions, ^{1}H and ^{19}F NMR spectra, GPC traces, FTIR spectra, DSC thermograms, WAXD patterns, SEM and TEM images, and TGA thermogram.

AUTHOR INFORMATION

Corresponding Author

Sanjay Rastogi - Physical Sciences and Engineering (PSE) Division, King Abdullah University of Science and Technology (KAUST), Thuwal 23955, Saudi Arabia.

Email: sanjay.rastogi@kaust.edu.sa

Authors

Yogesh Patil - Physical Sciences and Engineering (PSE) Division, King Abdullah University of Science and Technology (KAUST), Thuwal 23955, Saudi Arabia.

Email: yogesh.patil@kaust.edu.sa

Jiayi Zhao - Physical Sciences and Engineering (PSE) Division, King Abdullah University of Science and Technology (KAUST), Thuwal 23955, Saudi Arabia.

Email: jiayi.zhao@kaust.edu.sa

Bruno Ameduri - Institut Charles Gerhardt, CNRS, University of Montpellier, ENSCM, Montpellier, 34095, France.

Email: bruno.ameduri@enscm.fr

Author Contributions

The manuscript was written through the contributions of all authors. All authors have given approval to the final version of the manuscript.

Notes

The authors declare no competing financial interest.

ACKNOWLEDGMENT

This work was financially supported by the King Abdullah University of Science and Technology (KAUST).

REFERENCES

(1) Scheirs, J. Modern fluoropolymers: High-performance polymers for diverse applications. John Wiley & Sons Inc.: New York, 1997; pp-660.

(2) Ameduri, B. From Vinylidene Fluoride (VDF) to the Applications of VDF-Containing Polymers and Copolymers: Recent Developments and Future Trends. *Chem. Rev*. **2009**, *109*, 6632-6686.

(3) Ameduri, B.; Boutevin, B. Well-Architectured Fluoropolymers: Synthesis, Properties, and Applications. Elsevier: Amsterdam, 2004.

(4) Voet, V. S.; ten Brinke, G.; Loos, K. Well-defined copolymers based on poly(vinylidene fluoride): from preparation and phase separation to application. *J. Polym. Sci. Part A: Polym. Chem*. **2014**, *52*, 2861-2877.

(5) Smith, D. W.; Iacono, S. T.; Iyer, S. S. Handbook of Fluoropolymer Science and Technology, Wiley: New York, 2014; pp-646.

(6) Zapsas, G.; Patil, Y.; Gnanou, Y.; Ameduri, B.; Hadjichristidis, N. Poly(vinylidene fluoride)-based complex macromolecular architectures: From synthesis to properties and applications. *Prog. Polym*. Sci. **2020**, *104*, 101231.

(7) Gregorio, G Jr.; Cestari, M. Effect of crystallization temperature on the crystalline phase content and morphology of poly(vinylidene fluoride). *J. Polym. Sci. Part B Polym. Phys.* **1994**, *32*, 859-870.

(8) Martins, P.; Lopes, A.; Lanceros-Mendez, S. Electroactive phases of poly(vinylidene fluoride): Determination, processing, and applications. *Prog. Polym. Sci*. **2014**, *39*, 683-706.

(9) Ruan, R.; Yao, X.; Chang, Y.; Zhou, L.; Qin, G.; Zhang, X. Properties and Applications of the β Phase Poly(vinylidene fluoride). *Polymers* **2018**, *10*, 228.

(10) Guyomar, D.; Pruvost, S.; Sebald, G. Energy harvesting based on FE-FE transition in ferroelectric single crystals. *IEEE Trans. Ultrason. Ferroelectr. Freq. Control* **2008**, *55*, 279-285.

(11) Bar-Cohen, Y.; Zhang, Q. Electroactive Polymer Actuators and Sensors. *MRS Bulletin* **2008**, *33*, 173-181.

(12) Liu, Z. H.; Pan, C. T.; Lin, L. W.; Lai, H. W. Piezoelectric properties of PVDF/MWCNT nanofiber using near-field electrospinning. *Sens. Actuators* **2013**, *193*, 13-24.

(13) María, N.; Patil, Y.; Polymeropoulos, G.; Peshkov, A.; Rodionov, V.; Maiz, J.; Hadjichristidis, N.; Müller, A. J. PVDF)$_2$(PEO)$_2$ miktoarm star copolymers: Synthesis and isothermal crystallization leading to exclusive β-phase formation. *Eur. Polym. J.* **2022**, *179*, 111506.

(14) Lando, J. B.; Doll, W.W. The polymorphism of poly(vinylidene fluoride). I. The effect of head-to-head structure. *J. Macromol. Sci. Part B* **1968**, *2*, 205-218.

(15) Kepler, R. G.; Anderson, R. A. Piezoelectricity and pyroelectricity in polyvinylidene fluoride. *J. Appl. Phys*. **1978**, *49*, 4490-4494.

(16) Lovinger, A. J. Annealing of poly(vinylidene fluoride) and formation of a fifth phase. *Macromolecules* **1982**, *15*, 40-44.

(17) Salimi, A.; Yousefi, A. A. FTIR studies of beta-phase crystal formation in stretched PVDF films. *Polym. Test.* **2003**, *22*, 699-704.

(18) Pan, H.; Na, B.; Lv, R.; Li, C.; Zhu, J.; Yu, Z. Polar phase formation in poly(vinylidene fluoride) induced by melt annealing. *J. Polym. Sci. Part B: Polym. Phys.* **2012**, *50*, 1433-1437.

(19) Martins, P.; Nunes, J. S.; Hungerford, G.; Miranda, D.; Ferreira, A.; Sencadas, V.; Lanceros-Méndez, S. Local variation of the dielectric properties of poly(vinylidene fluoride) during the α- to β-phase transformation. *Phys. Lett. A* **2009,** *373*,177–180.

(20) Sencadas, V.; Gregorio Filho, R.; Lanceros-Mendez, S. Processing and characterization of a novel nonporous poly(vinylidene fluoride) films in the β phase. *J. Non-Cryst. Solids* **2006**, *352*, 2226-2229.

(21) Pan, H.; Na. B.; Lv. R.; Li. C.; Zhu, J.; Yu. Z. Polar Phase Formation in Poly(vinylidene fluoride) Induced by Melt Annealing. *J. Polym. Sci. Part B: Polym Phy.* **2012**, *50*, 1433-1437.

(22) Sajkiewicz, P. Crystallization behavior of poly(vinylidene fluoride). *Eur. Polym. J.* **1999**, *35*, 1581-1590.

(23) Al-Raheil, l. A.; Qudah, A. M. Thermal Behaviour and Annealing of Poly(viny1idene fluoride). *Polym. Int.* **1996**, *41*, 323-326.

(24) Marega, C.; Marigo, A. Influence of annealing and chain defects on the melting behavior of poly(vinylidene fluoride). *Eur. Polym. J.* **2003**, *39*, 1713-1720.

(25) Nakamura, K.; Sawai, D.; Watanabe, Y.; Taguchi, D.; Takahashi, Y.; Furukawa, T.; Kanamoto, T. Effect of Annealing on the Structure and Properties of Poly(vinylidene fluoride) β-Form Films. *J. Polym. Sci.: Part B: Polym. Phys.* **2003**, *41*, 1701-1712.

(26) Gradys, A.; Sajkiewicz, P.; Adamovsky, S.; Minakov, A.; Schick, C. Crystallization of poly(vinylidene fluoride) during ultra-fast cooling. *Thermochim. Acta*. **2007**, *461*, 153-157.

(27) Pérez, E.; Angulo, I.; Blázquez-Blázquez, E.; Cerrada, M. L. Characteristics of the non-isothermal and isothermal crystallization for the β polymorph in PVDF by fast scanning calorimetry. *Polymers* (Basel), **2020**, *12*, 2708.

(28) Yang, D.; Chen, Y. β-phase formation of poly (vinylidene fluoride) from the melt induced by quenching. *J. Mater. Sci. Lett*. **1987**, *6*, 599-603.

(29) Ma, W.; Zhang, J.; Chen, S.; Wang, X. Crystalline Phase Formation of Poly(vinylidene fluoride) from Tetrahydrofuran/ N,N-dimethylformamide Mixed Solutions. *J. Macromol. Sci., Part B: Phys.* **2008**, *47*, 434-449.

(30) Lederle, F.; Härter, C.; Beuermann, S. Inducing β phase crystallinity of PVDF homopolymer, blends and block copolymers by anti-solvent crystallization. *J. Fluor. Chem.* **2020**, *234*, 109522.

(31) Gregorio, R. Jr.; Chaves Pereira de Souza Nociti, N. Effect of PMMA addition on the solution crystallization of the alpha and beta phases of poly(vinylidene fluoride) (PVDF). *J. Phys. D Appl. Phys.* **1995**, *28*, 432.

(32) Hattori, T.; Kanaoka, M.; Ohigashi, H. Improved piezoelectricity in thick lamellar β-form crystals of poly (vinylidene fluoride) crystallized under high pressure. *J. Appl. Phys.* **1996**, *79*, 2016-2022.

(33) Zhong, G.; Zhang, L.; Su, R.; Wang, K.; Fong, H.; Zhu, L. Understanding polymorphism formation in electrospun fibers of immiscible poly (vinylidene fluoride) blends. *Polymer*, **2011**, *52*, 2228-2237.

(34) Sencadas, V.; Gregorio, R Jr.; Lanceros-Mendez, S. α to β Phase Transformation and Microstructural Changes of PVDF Films Induced by Uniaxial Stretch. *J. Macromol. Sci., Part B: Phys.* **2009**, *48*, 514-525.

(35) Gomes, J.; Nunes, J. S.; Sencadas, V.; Lanceros-Mendez, S. Influence of the β-phase content and degree of crystallinity on the piezo- and ferroelectric properties of poly(vinylidene fluoride). *Smart Mater. Struct.* **2010**, *19*, 065010.

(36) Imamura, R.; Silva, A. B.; Gregorio, R Jr. γ to β Phase Transformation Induced in Poly(vinylidene fluoride) by Stretching. *J. Appl. Polym. Sci.* **2008**, *110*, 3242-3246.

(37) Branciforti, M. C. Sencadas, V.; Lanceros-Mendez, S.; Gregorio, R Jr. New Technique of Processing Highly Oriented Poly(vinylidene fluoride) Films Exclusively in the β-Phase. *J. Polym. Sci.: Part B: Polym. Phys.* **2007**, *45*, 2793-2801.

(38) Mandal, D.; Kim, K. J.; Lee, J. S. Simple synthesis of palladium nanoparticles, β-phase formation, and the control of chain and dipole orientations in palladium doped poly(vinylidene fluoride) thin films. *Langmuir* **2012**, *28*, 10310-10317.

(39) Wolff, S.; Jirasek, F.; Beuermann, S.; Turk, M. Crystal phase transformation of α into β phase poly (vinylidene fluoride) via particle formation caused by rapid expansion of supercritical solutions. *RSC Adv.* **2015**, *5*, 66644-66649.

(40) Fan, Z.; Schwedes, M.; Schwaderer, J.; Beuermann, S.; Fischlschweiger, M. Molecular weight as a key for electroactive phase formation in poly(vinylidene fluoride). *Mater. Res. Lett*. **2022**, *10*, 271-277.

(41) Fischlschweiger, M.; Enders, S. Solid–liquid equilibria of crystalline and semi-crystalline monodisperse polymers, taking into account the molecular architecture by application of the lattice cluster theory. *Mol. Phys.* **2014**, *112*, 3109-3119.

(42) Fischlschweiger, M.; Enders, S. A theory for solubility of semicrystalline and branched polymers in one solvent. *Macromolecules* **2014**, *47*, 7625-7636.

(43) Fischlschweiger, M.; Enders, S. Thermodynamic principles for the design of polymers for drug formulations. *Annu. Rev. Chem. Biomol. Eng.* **2019**, *10*, 311-335.

(44) Boyer, C.; Valade, D.; Sauguet, L.; Ameduri, B.; Boutevin, B. Iodine Transfer Polymerization (ITP) of Vinylidene Fluoride (VDF). Influence of the Defect of VDF Chaining on the Control of ITP. *Macromolecules* **2005**, *38*, 10353-10362.

(45) Twum, E. B.; Gao, C.; Li, X.; McCord, E. F.; Fox, P. A.; Lyons, D. F.; Rinaldi, P. L. Characterization of the Chain-Ends and Branching Structures in Polyvinylidene Fluoride with Multidimensional NMR. *Macromolecules* **2012**, *45*, 5501−5512.

(46) Patro, T. U.; Mhalgi, M. V.; Khakhar, D. V.; Misra, A. Studies on poly(vinylidene fluoride)–clay nanocomposites: Effect of different clay modifiers. *Polymer* **2008**, *49*, 3486–3499.

(47) Adamson, N.; Glushenkov, A. M.; Lussini, V. C.; Fox, P. J.; Dicinoski, G. W.; Shapter, J. G.; Ellis, A. V. New developments in composites, copolymer technologies and processing techniques for flexible fluoropolymer piezoelectric generators for efficient energy harvesting. *Energy Environ. Sci*. **2019**, *12*, 1143-1176

(48) Chapron, D.; Rault, F.; Talbourdet, A.; Lemort, G,; Cochrane, C.; Bourson, P.; Devaux, E.; Campagne, C. In-situ Raman monitoring of the poly(vinylidene fluoride) crystalline structure during a melt-spinning process. *J. Raman Spectrosc*. **2021**, *52*, 1073-1079.

(49) Sherman, J. D.; Elloian. J.; Jadwiszczak, J.; Shepard, K. L. On the Temperature Dependence of the Piezoelectric Response of Prepoled Poly(vinylidene fluoride) Films. *ACS Appl. Polym. Mater*. **2020**, *2*, 5110–5120.

(50) Rault, F.; Chapron, D.; Talbourdet, A.; Cochrane, C.; Lemort, G.; Devaux, E.; Campagne, C.; Bourson, P. Interest of in Situ-Raman Spectroscopy in the Optimization of Piezoelectric Fibers for the Development of Energy Harvesters. *AUTEX2019 – 19th World Textile Conference on Textiles at the Crossroads*, 11-15 June **2019**, Ghent, Belgium.

(51) Satapathy, S.; Gupta, P. K.; Pawar, S.; Varma, K. B. R. Crystallization of β-phase Poly (vinylidene fluoride) films using dimethyl sulfoxide (DMSO) solvent and at suitable annealing condition. *arXiv preprint arXiv:0808.0419* **2008**.

(52) Pladis, P.; Alexopoulos, A. H.; Kiparissides, C. Mathematical Modeling and Simulation of Vinylidene Fluoride Emulsion Polymerization. *Ind. Eng. Chem. Res.* **2014**, *53*, 7352−7364.

(53) Gregorio, R Jr. Determination of the α, β, and γ Crystalline Phases of Poly(vinylidene fluoride) Films Prepared at Different Conditions. *J. Appl. Polym. Sci.* **2006**, *100*, 3272–3279.

(54) Martin, J.; Mijangos, C.; Sanz, A.; Ezquerra, T. A.; Nogales, A. Segmental Dynamics of Semicrystalline Poly(vinylidene fluoride) Nanorods. *Macromolecules* **2009**, *42*, 5395–5401

(55) Hou, C.; Zhang, W.; Dai, X.; Qiu, J.; Russell, T. P.; Sun, X.; Yan, S. Spatially Confined Fabrication of Polar Poly(Vinylidene Fluoride) Nanotubes. *Small* **2022**, *18*, 2205790-2205796.

(56) Dong, Y.; Wu, J.; Hu, J.; Yan, S.; Müller, A. J.; Sun, X. Thermal-Field-Tuned Heterogeneous Amorphous States of Poly(vinylidene fluoride) Films with Precise Transition from Nonpolar to Polar Phase. *Macromolecules* **2022**, *55*, 9671−9679.

(57) Mi, C.; Dong, Y.; Wang, S.; Li, H.; Zhu, L.; Sun, X.; Yan, S. Facile fabrication of ferroelectric poly(vinylidene fluoride) thin films with pure γ phase. *Chem. Commun*. **2022**, *58*, 9690-9693.

(58) Wunderlich, B. Crystal melting. *Macromol. Phys.* **1980**, *3*, 363.

(59) Goldbach, J. T.; Amin-Sanayei, R.; He, W.; Henry, J.; Kosar, W.; Lefebvre, A.; O'brien, G.; Vaessen, D.; Wood, K.; Zerafati, S. Commercial Synthesis and Applications of Poly(Vinylidene Fluoride). In *Fluorinated Polymer Vol. 2*: *Applications*; Ameduri, B., Sawada, H., Eds.; Royal Society of Chemistry: Cambridge, **2016**.

(60) Terzic, I.; Meereboer, N. L.; Loos, K. CuAAC click chemistry: a versatile approach towards PVDF-based block copolymers. *Polym. Chem*. **2018**, *00*, 1–7.

(61) Meereboer, N. L.; Terzic, I.; Saidi, S.; Hermida Merino, D.; Loos, K. Nanoconfinement-Induced β-Phase Formation Inside Poly(vinylidene fluoride)-Based Block Copolymers. *ACS Macro Lett.* **2018**, *7*, 863−867.

(62) Organ, S. J.; Keller, A. Solution crystallization of polyethylene at high temperatures Part 1 Lateral crystal habits. *J. Mater. Sci*. **1985**, *20*, 1571-1585.

(63) Ungar, G. "Self-Poisoning" of Crystal Growth Faces in Long Alkanes and Poly(Ethylene Oxide) Fractions. In: Dosière, M. (eds) Crystallization of Polymers. NATO ASI Series, vol 405. Springer, Dordrecht, 1993.

(64) Eid, N.; Gimello, O.; Bonnet, A.; Devisme, S.; Améduri, B. Chain-End Functionality: The Key Factor toward Fluoropolymer Thermal Stability. *Macromolecules* **2021**, *54*, 7690−7701.

(65) Rahul, M. T.; Kalarikkal, N.; Thomas, S.; Ameduri, B.; Rouxel, D.; Balakrishnan, R. Engineered Polymer Nanocomposites for Energy Harvesting Applications, Elsevier, **2022**.

(66) Vasic, N.; Steinmetz, J.; Görke, M.; Sinapius, M.; Hühne, C.; Garnweitner, G. Phase Transitions of Polarised PVDF Films in a Standard Curing Process for Composites. *Polymers* **2021**, *13*, 3900.

(67) Zhu, Y.; Huijian, Y.; Yang, L.; Jiang, L.; Zhen, L.; Huang, J.; Jiao, Z.; Sun, J. Effect of Annealing Temperatures and Time on Structural Evolution and Dielectric Properties of PVDF Films. *Polym. Polym. Compos*. **2016**, *24*, 167-172.

(68) Gradys, A.; Sajkiewicz, P. Determination of the melting enthalpy of β phase of poly(vinylidene fluoride). *e-Polymers* **2013**, *13*, 19.

(69) Inoue, M.; Tada, Y.; Suganuma, K.; Ishiguro, H. Thermal stability of poly(vinylidene fluoride) films pre-annealed at various temperatures. *Polym. Degrad. Stab*. **2007**, *92*, 1833-1840.

(70) Patil, Y.; Hori, H.; Tanaka, H.; Sakamoto, T.; Ameduri, B. First radical homopolymerization of 2-trifluoromethacrylic acid in water and study of the degradation of the resulting homopolymers. *Chem. Commun.* **2013**, *49*, 6662-6664.

(71) Korzeniowski, S. H.; Buck, R. C.; Newkold, R. M.; El kassmi, A.; Laganis, E.; Matsuoka, Y.; Dinelli, B.; Beauchet, S.; Adamsky, F.; Weilandt, K.; Soni, V.; Kapoor, D.; Gunasekar, P.; Malvasi, M.; Brinati, G.; Musio, S. A critical review of the application of polymer of low concern

regulatory criteria to fluoropolymers II: Fluoroplastics and fluoroelastomers. *Integr. Environ. Assess Manag.* **2023**, *19*, 326–354.

(72) Xiaoshi Qian, X.; Chen, X.; Zhu, L.; Zhang, Q. M. Fluoropolymer ferroelectrics: Multifunctional platform for polar-structured energy conversion. *Sci.* **2023**, *380*, 596.

(73) Glüge, J.; London, R.; Cousins, I. T.; DeWitt, J.; Goldenman, G.; Herzke, D.; Lohmann, R.; Miller, M.; Ng, C. A.; Patton, S.; Trier, X.; Wang, Z.; Scheringer, M. Information Requirements under the Essential-Use Concept: PFAS Case Studies. *Environ. Sci. Technol.* **2022**, *56*, 6232−6242.